



Dependence of dynamic strain ageing on strain amplitudes during the low-cycle fatigue of TP347H austenitic stainless steel at 550 °C



HongWei Zhou^{a,b,*}, YiZhu He^b, Mian Cui^b, YuWan Cen^c, JianQing Jiang^a

^a School of Materials Science and Engineering, Jiangsu Key Lab of Advanced Metallic Materials, Southeast University, Nanjing, 211189 Jiangsu, PR China

^b School of Materials Science and Engineering, Anhui Key Lab of Materials Science and Processing, Anhui University of Technology, Maanshan, 243002 Anhui, PR China

^c School of Mechanical Engineering, Anhui University of Technology, Maanshan, 243002 Anhui, PR China

ARTICLE INFO

Article history:

Received 1 March 2013

Received in revised form 4 July 2013

Accepted 6 July 2013

Available online 27 July 2013

Keywords:

TP347H austenitic stainless steel

Dynamic strain ageing

Low-cycle fatigue

Cyclic stress response

Dislocation structure

ABSTRACT

Low-cycle fatigue (LCF) tests are carried out on TP347H stainless steel at a strain rate of $8 \times 10^{-3} \text{ s}^{-1}$ with total strain amplitudes ($\Delta\epsilon_t/2$) of $\pm 0.4\%$ and $\pm 1.0\%$, at room temperature (RT) and 550 °C. It is found that the stress responses and dislocation structures under cyclic loading strongly depend on the value of strain amplitude at 550 °C. Compared with those at the same strain amplitude at RT, the material shows a rapid strain softening, and finally attains a stabilized state at $\Delta\epsilon_t/2 = \pm 0.4\%$ and 550 °C, but the one presents an anomalous behavior, i.e., first a rapid hardening to the maximum stress, followed by a reducing softening at $\Delta\epsilon_t/2 = \pm 1.0\%$ and 550 °C. More cells resulting from dislocation cross-slip and planar structures due to dynamic strain ageing (DSA) restricting cross-slip develop at low strain amplitude of $\pm 0.4\%$ at the first cycle. However, there are more complicated dislocation structures, such as cells, elongated cells, walls/channels and planar structures at $\Delta\epsilon_t/2 = \pm 1.0\%$. The observations of scanning electron microscopy (SEM) and transmission electron microscopy (TEM) exclude the effects of martensitic transformation, creep, oxidation, and precipitations on these stress responses and microstructure evolutions, which result from DSA appearing at 550 °C.

© 2013 Elsevier Ltd. All rights reserved.

1. Introduction

Austenitic stainless steels (ASS) have been widely used as a structural material in ultra-supercritical thermal power plants and petrochemical industries. It is also a candidate material for use in the cladding of nuclear fuel, heat exchangers, reactor pressure vessels and primary pipes for the next generation nuclear reactors. The components of high temperature systems are generally subjected to repeated thermal stresses due to the inevitable existence of temperature gradients, especially at the moments of start-ups or shut-downs, or during temperature transients. Hence, it is important to consider low-cycle fatigue (LCF) in the design of these components.

Many studies have been focused on LCF behavior of ASS at room temperature (RT) and elevated temperatures [1–10]. During LCF of ASS, there are many factors affecting the cyclic behaviors and microstructure evolutions, such as martensitic transformation, precipitation of carbides [1], and DSA [2]. At RT and temperatures below 100 °C, plasticity-induced martensitic transformation would occur under cyclic loading, the extent of which has been reported

to be associated with the amplitude of plastic deformation, as well as with the amount of cumulative plastic strain [3–7]. Plasticity-induced martensitic transformation results in cyclic hardening. It has been revealed that DSA during cyclic deformation and monotonic tensile loading at elevated temperatures between 250 °C and 650 °C usually has a significant influence on the stress response, LCF life, and microstructures [2,8] of ASS. It is reported that the regime of DSA under LCF loading is consistent with that in tensile loading [9]. DSA is manifested in the form of serrated yielding on the stress–strain hysteresis loops, the negative temperature dependence of cyclic peak stress, the negative temperature dependence of softening ratio, the negative strain rate sensitivity [9]. Even though serrations are believed to be one of the manifestations of DSA, recent studies on cyclically loaded 316L(N) have found that DSA occurs before serrations occurs [2,10].

In the DSA regime, dislocation structures under cyclic deformation are different from those in the no-DSA regime, due to the strong interactions between dislocations and impurity atoms such as C or N in the temperature range of 250–450 °C, Cr at higher temperature 450–650 °C [2,11,12]. Under cyclic loading, dislocation structures change from planar structures in the DSA regime to cell ones in the no-DSA regime. In general, there are two types of planar structures observed in the DSA regime, that is, planar slip bands [8,9,13,14] and corduroy structures, among which the corduroy structures have been investigated in vacuum at

* Corresponding author at: School of Materials Science and Engineering, Anhui Key Lab of Materials Science and Processing, Anhui University of Technology, Maanshan, 243002 Anhui, PR China. Tel.: +86 555 2311871; fax: +86 555 2311570.

E-mail addresses: zzzhw.1@gmail.com (H. Zhou), heyizhu@ahut.edu.cn (Y. He).

250–450 °C [15] and then recently found in air at 300 °C during cyclic loading [16].

In the medium temperature range from 250 to 450 °C, Suzuki atmospheres of solute atoms [11,16], or Snoek atmospheres characteristic of short-range-order (SRO) restrict the dislocation cross-slip [17], resulting in more planar character of dislocation structures. Cr solute atom atmospheres in a low nitrogen ASS or Cr–N SRO [13,18] in a high nitrogen 316 ASS effectively lock dislocations in the high temperature range 500–650 °C, which results in dislocation gliding on particular planes, manifested as planar structures.

Solute atom atmospheres effectively lock dislocations, resulting in higher immobile dislocation density and enhancing the degree of inhomogeneity of deformation by the solute locking of slow moving dislocations between planar slip bands during LCF [7,9]. The planar microstructures due to DSA are responsible for cyclic hardening during the primary stress response stages and secondary cyclic hardening at the last stages on the cyclic stress responses. It has been reported that DSA reduces the lifetime of LCF due to the DSA inducing cyclic hardening, which accelerates crack initiation and propagation [7,9,14].

According to these studies [7,9,14], simple dislocation structures develop, i.e., planar structures in the DSA regime and cell ones in the no-DSA regime. It is well known that the dislocation structures depend on strain amplitude in LCF at RT [19]. In each regime of cyclic stress–strain curve a dominant dislocation structure was found [20]: planar dislocation arrays arranged in sheets at ε_{ap} (plastic strain amplitude) <0.01%, imperfect vein structure with persistent slip bands at ε_{ap} between 0.01% and 0.1%, and cells and wall structures at ε_{ap} > 0.1%.

In this study, we focus on the effects of total strain amplitude on the LCF of ASS at 550 °C where DSA happens. For the purpose of comparison, LCF tests in the no-DSA regime at RT are also carried out.

2. Experiment

The investigated materials were commercial niobium-stabilized TP347H austenitic stainless steel pipes for power plants. All of the specimens were solution-treated at 1100 °C for 10 min followed by water quenching. The chemical composition of the alloy is shown in Table 1. A microstructure with prior austenite grains with the size of nearly 50 μm is shown in Fig. 1. Tensile tests were conducted at room temperature (RT) and 550 °C with an initial constant strain rate of $1 \times 10^{-4} \text{ s}^{-1}$.

The dog-bone specimens with a 28 mm gauge length and 7 mm gauge diameter were machined. The specimen surface was polished along the longitudinal direction with the emery paper down to #1000 in order to remove surface defects, such as machining marks and scratches. All the tests were carried out in air under a fully-reversed, total axial strain control mode at the low total strain amplitude $\Delta\varepsilon_t/2 = \pm 0.4\%$ and high $\Delta\varepsilon_t/2 = \pm 1.0\%$, where $\Delta\varepsilon_t$ is the total strain amplitude, at a constant strain rate of $8 \times 10^{-3} \text{ s}^{-1}$ at RT and 550 °C. A symmetrical triangular strain–time waveform was employed, using an IEHF-EM200k1-070-0A testing system (Shimadzu) controlled by an extensometer (Epsilon). The temperature variation along the gauge length of the specimen in a three-zone-furnace did not exceed ± 2 °C.

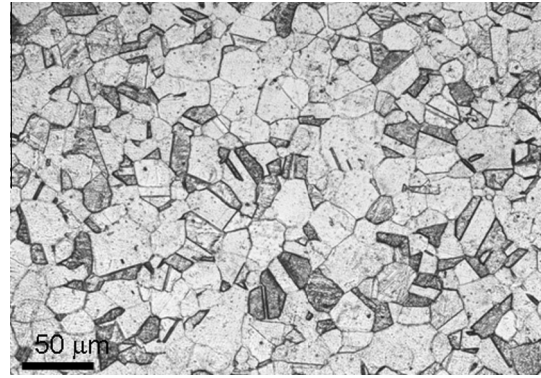


Fig. 1. Optical micrograph of TP347H steel.

JSM-6360LV Scanning Electron Microscopy (SEM) was applied to examine the fracture surface of the specimens. Transmission Electron Microscopy (TEM) examinations were conducted with a Philips Tecnai12 microscope, operating at 200 kV. TEM was used to investigate the evolution of dislocation structures and carbides under LCF conditions at RT and 550 °C. Samples for TEM were obtained from thin slices cut at a distance of 2 mm away from the fracture surface. The slices were electrolytically polished using a double jet device with an electrolyte solution of 80 ml of methanol and 20 ml of perchloric acid at -30 °C.

3. Results

3.1. Tensile and hysteresis loops

The typical engineering stress–strain curves for TP347H steel tested at RT and 550 °C are shown in Fig. 2. As seen from Fig. 2, serrations on the stress–strain curves occur at 550 °C, while this phenomenon are absent in the whole range of the strain at RT. According to previous descriptions of the oscillations [21], the serrations at 550 °C observed in Fig. 2 appear to be a mixture of two types A and B. Type A serrations of lower frequency occur due to periodic locking of dislocations and show an abrupt rise in the load followed by discontinuous drops to or below the general level of the stress–strain curves. Type B serrations of high frequency oscillate about the general level of the stress–strain curves, which occur in quick succession due to discontinuous band propagation arising from the DSA of the moving dislocations within the Lüders band. The occurrence of the serrations as a result of the interactions between Cr atoms and dislocations is a typical DSA manifestation in the studied steel at 550 °C. In the present study, serrated yielding was not observed in the stress–strain hysteresis loops during LCF deformation, as shown in Fig. 3. This absence is thought to be a result that the strain amplitude of $\pm 0.4\%$ and $\pm 1.0\%$ used in LCF tests is relatively smaller compared with the critical strain that is necessary for serrated yielding to occur. According to other studies about 316L ASS [22], although no serrations occur on the loops, but DSA happens at 550 °C and at strain rate range $1 \times 10^{-4} \text{ s}^{-1}$ – $1 \times 10^{-2} \text{ s}^{-1}$. In the following sections, DSA will be proved to occur in other ways at 550 °C.

Table 1
Chemical composition of TP347H (wt.%).

Element	C	N	P	S	Cr	Ni	Mo	Mn	Si	Nb	Fe
wt.%	0.05	0.016	0.0172	0.006	18.50	11.44	0.940	1.11	0.45	0.726	Balance

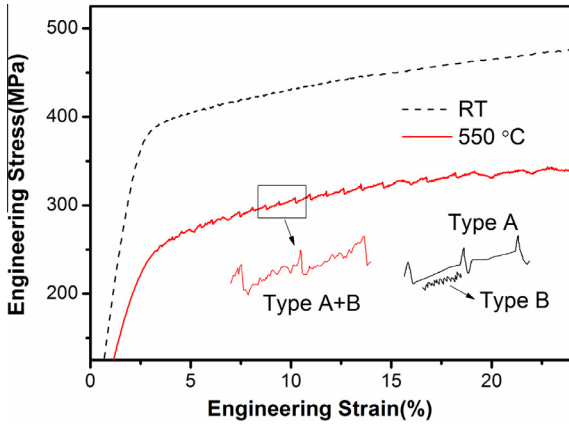


Fig. 2. Tensile stress–strain curves.

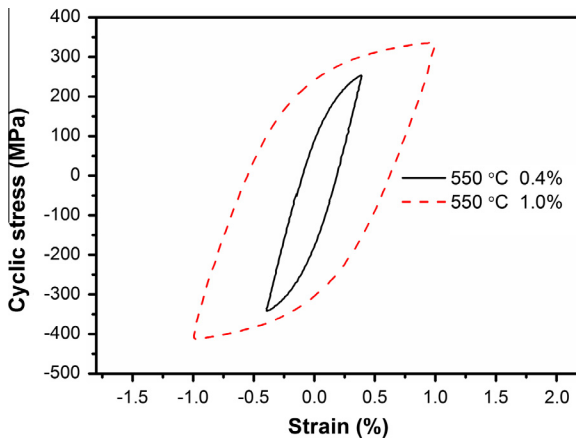


Fig. 3. Hysteresis loops at $\Delta\epsilon_f/2 = \pm 0.4\%$ and $\pm 1.0\%$ at $550\text{ }^\circ\text{C}$.

3.2. Cyclic stress response

The cyclic stress response at RT and $550\text{ }^\circ\text{C}$ is shown in Fig. 4. It can be seen that there are two typical stages for all conditions except at $\Delta\epsilon_f/2 = \pm 0.4\%$, an initial cyclic hardening appeared at the several cycles, followed by a continuous cyclic softening until a rapid stress drop due to crack initiation and growth. It is interesting

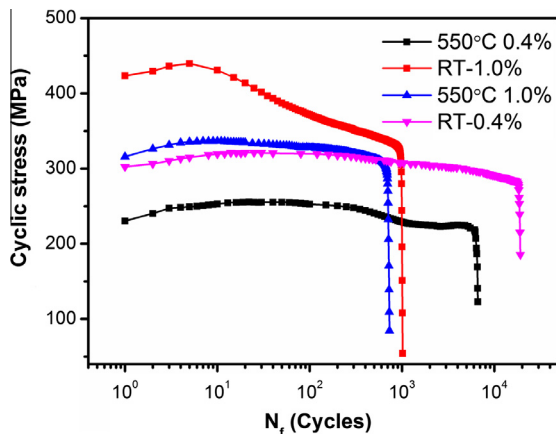


Fig. 4. Cyclic stress–strain responses at RT and $550\text{ }^\circ\text{C}$ with the different strain amplitude.

to note that the specimen at $\Delta\epsilon_f/2 = \pm 0.4\%$ and $550\text{ }^\circ\text{C}$ shows a slow initial strain hardening, followed by a strain softening, and finally a stabilized state.

At RT, cyclic softening is more remarkable at higher strain amplitude of $\pm 1.0\%$ than that at $\Delta\epsilon_f/2 = \pm 0.4\%$. However, rather than at $\Delta\epsilon_f/2 = \pm 1.0\%$, the trend of cyclic softening at low strain amplitude of $\pm 0.4\%$ is more pronounced at $550\text{ }^\circ\text{C}$ after an initial hardening. At the same strain amplitude of $\pm 0.4\%$, softening at $550\text{ }^\circ\text{C}$ is more than that at RT. However, compared with that at RT and the same strain amplitude of $\pm 1.0\%$, the cyclic stress response at $550\text{ }^\circ\text{C}$ shows first a rapid hardening to the maximum stress, followed by a reducing softening through the LCF life. It is worth pointing out that a stabilized state develops after a strain softening at $\Delta\epsilon_f/2 = \pm 0.4\%$ and RT, which indicates that some charging microstructures under LCF restrain the strain softening. Martensitic transformation, DSA, and carbides precipitations could result in a primary rapid hardening, then a reducing strain softening, and finally a secondary hardening.

Fig. 4 also presents that the lifetime of the specimens at $550\text{ }^\circ\text{C}$ in the DAS regime is lower than that at RT and at the same strain amplitude, which agrees with other reports that DSA reduces the LCF life. However oxidation and creep also affect the LCF. These will be distinguished by means of SEM and TEM in the following sections.

3.3. Fracture features

Fig. 5 shows that fatigue cracks in all tested samples were initiated at the slip bands connected to the specimen free surface instead of the interior of the specimen, where there is no pronounced effect of oxidation. Crack propagation is transgranular under all LCF conditions, evidenced by striations on the fracture surface in Fig. 5c. At the same time, there is no evidence of intergranular damage which could be induced by creep. The sudden fracture region exhibits ductile characteristic of the steel, as shown in Fig. 5d. By means of fracture morphology, it may be to rule out the effect of oxidation and creep, consequently the reducing lifetime at $550\text{ }^\circ\text{C}$ should result from the effect of DSA, which lead to cyclic hardening, accelerates crack propagation, reducing the LCF life.

3.4. Dislocation microstructure

Figs. 6 and 7 present dislocation structures under cyclic loading at different strain amplitudes at RT. At $\Delta\epsilon_f/2 = \pm 0.4\%$, dislocation structures are characteristic of planar slip, i.e. stacking faults in Figs. 6a and b, which are due to low stacking fault energy of austenitic steels. There are many dislocation pile-ups in Figs. 6c and d. Because of low strain amplitude, no cell structures are formed. In contrast, well-defined cell structures develop at $\Delta\epsilon_f/2 = \pm 1.0\%$ in Fig. 7a. Dislocations gather in the cell walls, and the density of dislocation are very low within cells, as shown in Figs. 7a and b. Stacking faults are also formed near the grain boundary in Fig. 7c, and twins appear in Fig. 7d.

Martensite is not found at all strain amplitudes at RT, since cyclic loading does not satisfy the critical condition for strain inducing martensitic transformation. According to the literature [23], M_d in ASS is about $100\text{ }^\circ\text{C}$, where M_d is the maximum temperature at which the transformation can be induced by mechanical loading in austenitic stainless steels. As a result, martensite will be not formed at $550\text{ }^\circ\text{C}$.

It is clear that microstructures deeply depend on strain amplitudes under cyclic loading at $550\text{ }^\circ\text{C}$, as shown in Figs. 8 and 9. No carbide precipitates are found at high temperature of $550\text{ }^\circ\text{C}$. Firstly, the duration of LCF tests is too short to precipitate for carbides. At the same time, because of low content of carbon in ASS,

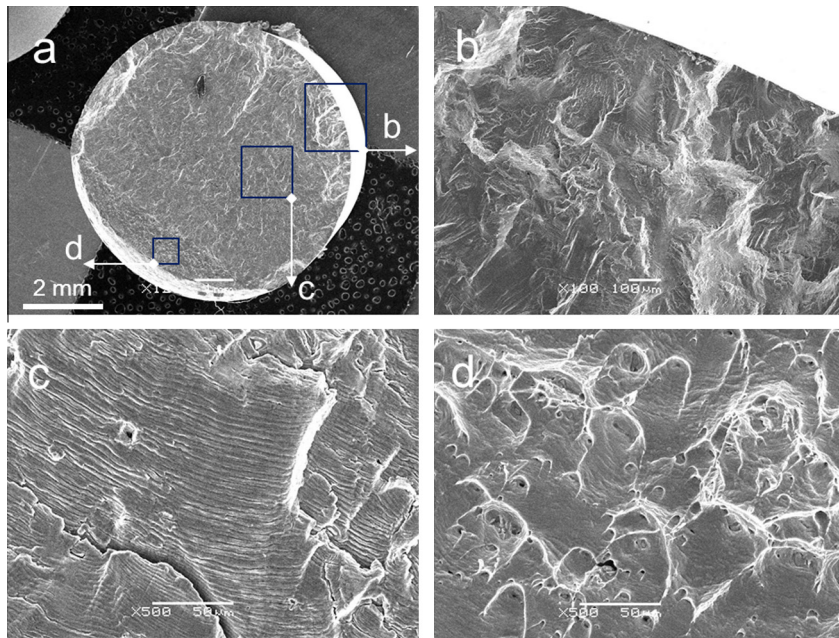


Fig. 5. SEM micrographs of fracture at 550 °C with $\Delta\epsilon_t/2 = \pm 0.4\%$ (a) whole view of fracture, (b) crack initiation, (c) striations and (d) dimple fracture.

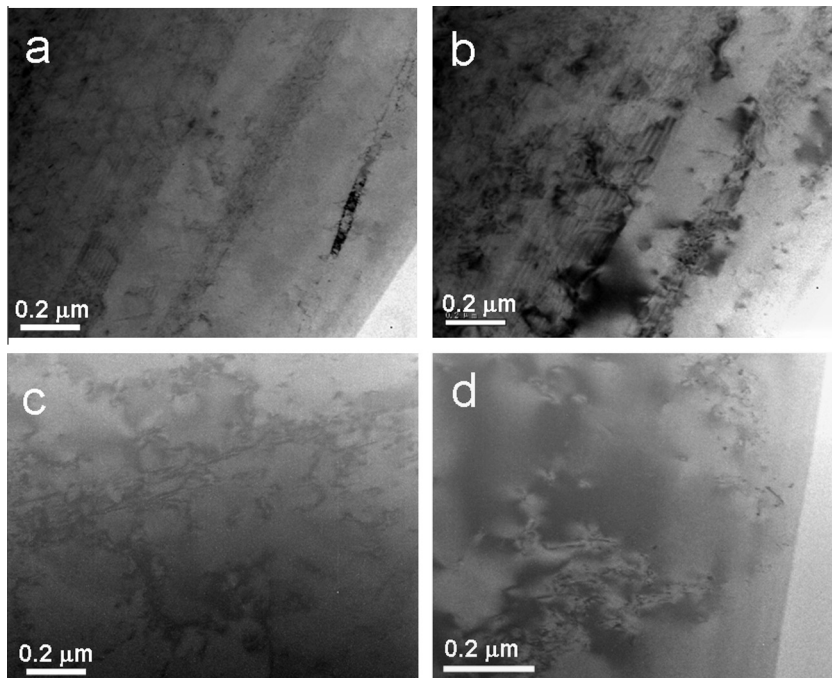


Fig. 6. TEM micrographs of the sample under LCF at $\Delta\epsilon_t/2 = \pm 0.4\%$ and RT (a) and (b) stacking faults, (c and d) dislocations pile-ups.

little carbides precipitate, while precipitates are often formed in ferritic/martensitic steels with high content of carbon in LCF at high temperature [24,25]. In the recent study of 316LN ASS, extensive carbide precipitates, $M_{23}C_6$ with high chromium content, were observed under thermo-mechanical fatigue (TMF) loading in the range of 300–650 °C in compared to isothermal LCF at the peak temperature. The carbide precipitates were believed to be partly responsible for the enhanced stress response obtained under TMF in comparison with isothermal LCF. The mechanism of precipitation under TMF is not clear. These observations show that rather than plasticity-induced martensitic transformation and carbide precipitates, microstructure evolutions at 550 °C should be respon-

sible for cyclic hardening, reducing softening at high $\Delta\epsilon_t$ and a stabilized state at low $\Delta\epsilon_t$.

As can be seen in Fig. 8a and b, incomplete cell structures are observed at $\Delta\epsilon_t/2 = \pm 0.4\%$. At the same time, Fig. 8c and d shows that planar slip bands are formed and many dislocation pile-ups are observed near planar slip bands. A cell structure results from the dislocation cross-slip, while planar structure develops due to DSA restricting cross-slip.

There are complicated deformation substructures at $\Delta\epsilon_t/2 = \pm 1.0\%$, i.e. planar slip bands in Fig. 9a and b, dislocation tangles in Fig. 9c, elongated cells and planar structures in Fig. 9d, a complex of planar structures and wall/channel in Fig. 9e. It can

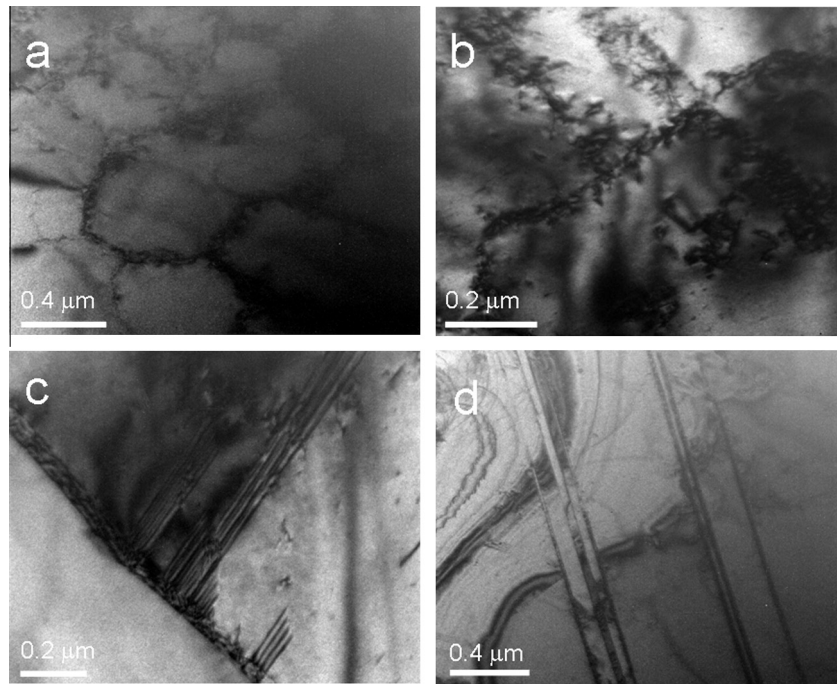


Fig. 7. TEM micrographs of the sample under LCF at $\Delta\epsilon_i/2 = \pm 1.0\%$ and RT (a) and (b) Cells, (c) stacking faults and (d) twins.

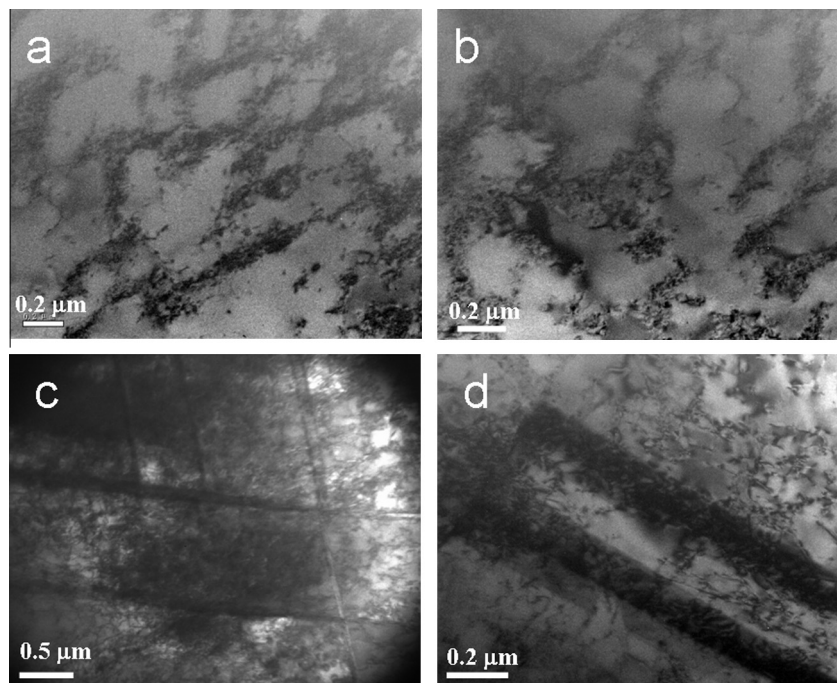


Fig. 8. TEM micrographs of the sample under LCF at $\Delta\epsilon_i/2 = \pm 0.4\%$ and 550 °C (a) and (b) cells, (c) planar structures and (d) planar structures and pile-ups.

be seen that the account of planar structures due to interaction between dislocations and solute atoms are more than those at $\Delta\epsilon_i/2 = \pm 0.4\%$, indicating that the effects of DSA are more pronounced at high strain amplitude. The wall/channel structures, which are often observed in 316L steel under loading at RT, develop between planar slip bands. The dislocation density within the walls is much higher than that within the channels, which creates high plastic incompatibilities. These observed dislocation structures are different from those in other austenitic steels, i.e. 316L, under cyclic deformation in the DSA regime.

Planar slip bands segregate the wall/channel structures shown in Fig. 9e, indicating that dislocations in wall/channel are unable to glide through planar structures, while planar slip bands can pass through the grain boundary in Fig. 9b, which is suggested that planar structures are very stable. This may be attributed to that DSA effectively restricts dislocation cross-slip, dislocation only gliding on particular planes. Once planar structures are formed, they can act as obstacles to dislocation movement, which in turn results in the hardening effect of the material. From Fig. 9c and d, it can be seen that the dislocation density is also higher due to solute atom

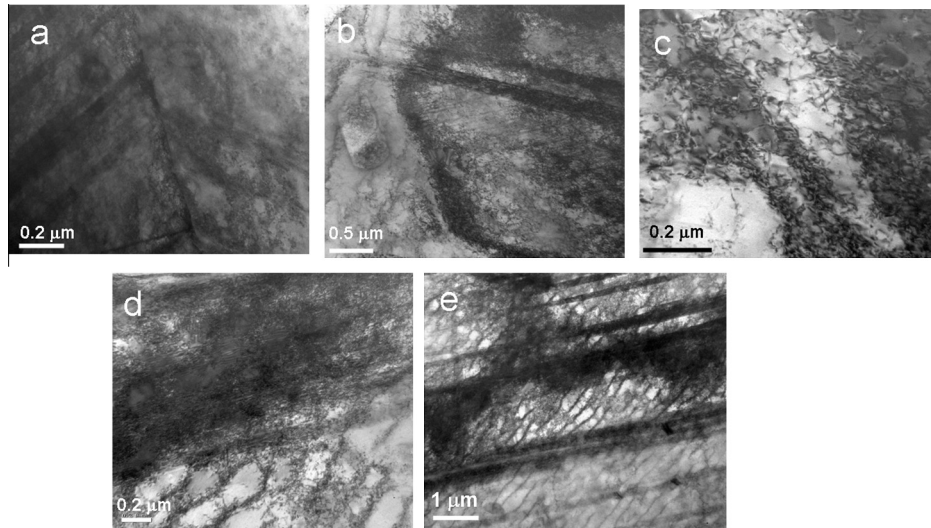


Fig. 9. TEM micrographs of the sample under LCF at $\Delta\varepsilon_t/2 = \pm 1.0\%$ and $550\text{ }^\circ\text{C}$ (a and b) planar structures, (c) dislocations tangled, (d) cells and planar structures, (e) complicated dislocation structures, i.e., wall/channel, cells, and elongated cells and planar structures.

atmospheres effectively locking than that at $550\text{ }^\circ\text{C}$ with $\Delta\varepsilon_t/2 = \pm 0.4\%$ and RT with $\Delta\varepsilon_t/2 = \pm 1.0\%$.

4. Discussion

TP347H steels have shown a primary cyclic hardening followed by a cyclic softening to sample failure, except that a stabilized state developing after a strain softening at $\Delta\varepsilon_t/2 = \pm 0.4\%$ at $550\text{ }^\circ\text{C}$. The sample at high strain amplitude is characteristic of an anomalous primary hardening and then reducing cyclic softening at $550\text{ }^\circ\text{C}$, compared to that at the same strain amplitude at RT. DSA mainly contributes to cyclic hardening, reducing softening at a high $\Delta\varepsilon_t$ and a stabilized state at low $\Delta\varepsilon_t$ and $550\text{ }^\circ\text{C}$, rather than plasticity-induced martensitic transformation and carbide precipitates.

Some studies [26] have shown that the microstructure of austenitic steel during strain-controlled cyclic loading with strain amplitude of $\pm 0.7\%$ at RT evolves from a planar dislocation structure into wall/channel and cell structures as a function of the number of cycles. In the present study, the mixture of dislocation structures also reserves the structures evolution history. The formation of cells and elongated cell structures shown in Fig. 9d may be mainly caused by two factors [20,26,27]. One is the subdivision of grains by dominant slip systems during the first several cycles. The other is the activation of cross slip and secondary slip systems with the increasing of cycles.

At RT and at high strain amplitude of $\pm 1.0\%$, cells, a lower energy structure due to mutual annihilation of dislocations by means of cross-slip and secondary slip systems, are responsible for rapid cyclic softening, while at low strain amplitude of $\pm 0.4\%$, planar structures, i.e. twins and stacking fault, and dislocation pile-ups instead of cells, result in more gradual cyclic softening compared to $\Delta\varepsilon_t/2 = \pm 1.0\%$. Dislocation rearrangement to cells easily formed at high strain amplitude is in accordance with the previous studies [19,20].

In present study, stacking faults are only observed in the samples under LCF at RT, rather than at $550\text{ }^\circ\text{C}$. Previous results [2,11,12] show the existence of two temperature regimes in terms of DSA, the first of which corresponds to a range ($250\text{--}450\text{ }^\circ\text{C}$) where DSA enhances planar slip in relation to carbon segregation on stacking faults, while the second regime ($450\text{--}700\text{ }^\circ\text{C}$) is associated with a DSA mechanism of Cr atoms locking dislocations. This is consistent with the result that stacking fault energy will rise

with the temperature and disappear at temperature higher than $450\text{ }^\circ\text{C}$. Consequently, Cr atoms locking dislocations is the DSA mechanism for the present work at $550\text{ }^\circ\text{C}$.

At high temperatures, edge dislocation climbing and screw dislocation sliding are more effectively activated under cyclic loading, dislocations move and annihilate with the opposite sign dislocation, resulting in dynamic recovery, i.e. formation of cells and sub-grains, which result in strain softening. Just as the tendency of cyclic response at RT and $\Delta\varepsilon_t/2 = \pm 1.0\%$, the low energy cell structures are also responsible for rapid cyclic softening at $550\text{ }^\circ\text{C}$ at $\Delta\varepsilon_t/2 = \pm 0.4\%$ compared with the gradual softening at the same strain amplitude at RT and the same temperature at $\Delta\varepsilon_t/2 = \pm 1.0\%$. This also reveals that at initial cycles, strain amplitude of $\pm 0.4\%$ may be so low that the effects of DSA are weak at $550\text{ }^\circ\text{C}$. With the accumulation of strain, the effect of DSA becomes stronger, restricting the cross-slip and planar structure has been observed in Fig. 8c and b. Once DSA solute atom atmospheres effectively locking dislocations result in higher immobile dislocation density and planar structures result in plastic incompatibilities, which compensates for the structure discovery due to high temperature. When the dislocation breeding and annihilation maintain a balance, a stabilized cyclic state arrives in Fig. 4c.

At high strain amplitude $\Delta\varepsilon_t/2 = \pm 1.0\%$ at $550\text{ }^\circ\text{C}$, an anomalous initial hardening and then reducing cyclic softening at $550\text{ }^\circ\text{C}$, compared with the same strain amplitude at RT, which indicates that DSA effectively occurs throughout the LCF life. Therefore, the planar-slip resulting from effective DSA mechanism, and the significant cross-slip due to high temperature, simultaneously happen. This indicates that the cyclic stress response is governed by two competitive processes, hardening from DSA resulting in structure incompatibilities and higher immobile dislocation density and softening from cell structures with low dislocation intensity. At the anomalous primary hardening stage, planar-slip is dominant and dislocation planarity appears in Fig. 9a and b, while at the cyclic softening stage following the maximum cyclic hardening stress, cross-slip is dominant, and cells and wall/channel structures are formed. However in this stage DSA still works, reducing the extent of cyclic softening compared to room temperature. Consequently, more complicated dislocation structures are formed, i.e. cells, elongated cells and wall/channel structures are embedded in planar structures compared to those at strain amplitude $\pm 0.4\%$, shown in Fig. 9e. It is well known that planar structures is due to solute

atoms strongly locking dislocations, which keeps dislocation gliding on particular planes. As for wall/channel structures, the activation of secondary slip planes strengthen interactions between dislocations which are responsible for the formation of dislocation-dense walls, while screw dislocations annihilate opposite sign screw dislocations and shorten edge dislocations in primary slip planes which result in dislocation-free channels [26,27], as shown in Fig. 9e.

5. Conclusion

Low-cycle fatigue (LCF) tests were carried out on TP347H stainless steel at a strain rate of $8 \times 10^{-3} \text{ s}^{-1}$ and strain amplitude of $\pm 0.4\%$ and $\pm 1.0\%$, at room temperature (RT) and 550°C . DSA widely depends on strain amplitude under cyclic loading at 550°C , and dislocation structures are related with the stress responses.

- The material under LCF at low strain amplitude of $\pm 0.4\%$ and 550°C shows a slow initial strain hardening, followed by a strain softening, and finally a stabilized state. While the material at high strain amplitude of $\pm 1.0\%$ is catachrestic of an anomalous primary hardening and then reducing softening through the LCF life, compared with that at RT. These responses at different amplitude at 550°C are found to be related with the DSA hardening mechanism which is manifested of planar dislocation structures.
- At low strain amplitude of $\pm 0.4\%$, the tendency for planar structures due to dislocation planar-slip during LCF is extended to higher cycle number.
- At high strain amplitude, two main types of dislocation structures are formed, the first of which is planar structures resulting from, and the second includes cells, elongated cells and wall/channel structures due to cross-slip and secondary slip systems.

Acknowledgements

This work was financially supported by The National High Technology Research and Development Program of China (863 Program, Grant No. 2009AA044802), and Program for Innovative Research Team in Anhui University of Technology.

References

- [1] Nagesha A, Kannan R, Parameswaran P, Sandhya R, Rao K, Singh V. A comparative study of isothermal and thermomechanical fatigue on type 316L (N) austenitic stainless steel. *Mater Sci Eng A* 2010;527:5969–75.
- [2] Hong SG, Lee SB. Mechanism of dynamic strain aging and characterization of its effect on the low-cycle fatigue behavior in type 316L stainless steel. *J Nucl Mater* 2005;340:307–14.
- [3] Smaga M, Walther F, Eifler D. Deformation-induced martensitic transformation in metastable austenitic steels. *Mater Sci Eng A* 2008;483–484:394–7.
- [4] Ye D, Matsuoka S, Nagashima N, Suzuki N. The low-cycle fatigue, deformation and final fracture behaviour of an austenitic stainless steel. *Mater Sci Eng A* 2006;415:104–17.
- [5] Hong SG, Lee SB, Byun TS. Temperature effect on the low-cycle fatigue behavior of type 316L stainless steel: cyclic non-stabilization and an invariable fatigue parameter. *Mater Sci Eng A* 2007;457:139–47.
- [6] Taheri S, Hauet A, Taleb L, Kpodekon C. Micro-macro investigations about the fatigue behavior of pre-hardened 304L steel. *Int J Plasticity* 2011;27:1981–2004.
- [7] Srinivasan VS, Sandhya R, Bhanu Sankara Rao K, Mannan SL, Raghavan KS. Effects of temperature on the low cycle fatigue behaviour of nitrogen alloyed type 316L stainless steel. *Int J Fatigue* 1991;13:471–8.
- [8] Yu D, Yu W, Chen G, Jin F, Chen X. Role of dynamic strain aging in the tensile property, cyclic deformation and fatigue behavior of Z2CND18.12N stainless steel between 293 K and 723 K. *Mater Sci Eng A* 2012;558:730–6.
- [9] Hong SG, Lee SB. Dynamic strain aging under tensile and LCF loading conditions, and their comparison in cold worked 316L stainless steel. *J Nucl Mater* 2004;328:232–42.
- [10] Srinivasan VS, Sandhya R, Valsan M, Rao KBS, Mannan SL, Sastry DH. The influence of dynamic strain ageing on stress response and strain-life relationship in low cycle fatigue of 316L(N) stainless steel. *Scripta Mater* 1997;37:1593–8.
- [11] Gentet D, Feaugas X, Risbet M, Lejeail Y, Pilvin P. Several aspects of the temperature history in relation to the cyclic behaviour of an austenitic stainless steel. *Mater Sci Eng A* 2011;528:7696–707.
- [12] Mannan S, Samuel K, Rodriguez P. Dynamic strain ageing in type 316 stainless steel. *Trans Indian Inst Metals* 1983;36:313–20.
- [13] Srinivasan VS, Valsan M, Sandhya R, Bhanu Sankara Rao K, Mannan SL, Sastry DH. High temperature time-dependent low cycle fatigue behaviour of a type 316L(N) stainless steel. *Int J Fatigue* 1999;21:11–21.
- [14] Meng LJ, Sun J, Xing H, Yu WW, Xue F. Study of low-cycle fatigue of AL6XN austenitic stainless steel. *Nucl Eng Des* 2011;241:2839–42.
- [15] Gerland M, Alain R, Ait Saadi B, Mendez J. Low cycle fatigue behaviour in vacuum of a 316L-type austenitic stainless steel between 20 and 600°C . Part II: Dislocation structure evolution and correlation with cyclic behaviour. *Mater Sci Eng A* 1997;229:68–86.
- [16] Pham MS, Holdsworth SR. Dynamic strain ageing of AISI 316L during cyclic loading at 300°C : mechanism, evolution, and its effects. *Mater Sci Eng A* 2012;556:122–33.
- [17] Karlsen W, Ivanchenko M, Ehrstén U, Yagodzinskyy Y, Hänninen H. Microstructural manifestation of dynamic strain aging in AISI 316 stainless steel. *J Nucl Mater* 2009;395:156–61.
- [18] Kim DW, Ryu WS, Hong JH, Choi SK. Effect of nitrogen on high temperature low cycle fatigue behaviors in type 316L stainless steel. *J Nucl Mater* 1998;254:226–33.
- [19] Mayama T, Sasaki K, Kuroda M. Quantitative evaluations for strain amplitude dependent organization of dislocation structures due to cyclic plasticity in austenitic stainless steel 316L. *Acta Mater* 2008;56:2735–43.
- [20] Obrtlík K, Kruml T, Polák J. Dislocation structures in 316L stainless steel cycled with plastic strain amplitudes over a wide interval. *Mater Sci Eng A* 1994;187:1–9.
- [21] Rodriguez P. Serrated plastic flow. *B Mater Sci* 1984;6:653–63.
- [22] Hong SG, Lee KO, Lee SB. Dynamic strain aging effect on the fatigue resistance of type 316L stainless steel. *Int J Fatigue* 2005;27:1420–4.
- [23] Baudry G, Pineau A. Influence of strain-induced martensitic transformation on the low-cycle fatigue behavior of a stainless steel. *Mater Sci Eng* 1977;28:229–42.
- [24] Zhou H, Wei, He Y, Zhu, Zhang H, Cen Y, et al. Influence of dynamic strain aging pre-treatment on the low-cycle fatigue behavior of modified 9Cr–1Mo steel. *Int J Fatigue* 2013;47:83–9.
- [25] Shankar V, Valsan M, Rao KBS, Kannan R, Mannan SL, Pathak SD. Low cycle fatigue behavior and microstructural evolution of modified 9Cr–1Mo ferritic steel. *Mater Sci Eng A* 2006;437:413–22.
- [26] Pham MS, Solenthaler C, Janssens KGF, Holdsworth SR. Dislocation structure evolution and its effects on cyclic deformation response of AISI 316L stainless steel. *Mater Sci Eng A* 2011;528:3261–9.
- [27] Li Y, Laird C. Cyclic response and dislocation structures of AISI 316L stainless steel. Part 2: Polycrystals fatigued at intermediate strain amplitude. *Mater Sci Eng A* 1994;186:87–103.